1. De Vaucouleurs, G., *Physics of the Planet Mars*, Faber and Faber, London, 1952.
2. De Vaucoulehrs, G., A low-resolution photometric map of Mars. *Icarus*, 1967, **7**, 310–349.
3. Kieffer, H. H., Martin, T. Z., Peterfreund, A. R., Jakosky, B. M., Miner, E. D. and Palluconi, F. D., Thermal and albedo mapping of Mars during the viking primary mission. *J. Geophys. Res.*, 1977, **82**, 4249–4292.
4. Christensen, P. R., Global albedo variations on Mars: implications for active aeolian transport, deposition and erosion. *J. Geophys. Res.*, 1988, **93**, 7611–7624.
5. Bibring, J.-P. *et al.*, ISM observations of Mars and Phobos: First results. Proceedings of the 20th Lunar Planetary Science Conference, 1990, pp. 461–471.
6. Mustard, J. E. *et al.*, The surface of Syrtis Major: composition of the volcanic substrate and mixing with altered dust and soil. *J. Geophys. Res.*, 1993, **98**, 3387–3400.
7. Soderblom, A., The composition and surface mineralogy of the Martian surface from spectroscopic observations: 0.3 μm to 50 μm, in Mars (eds Kieffer, H. H. *et al.*), Univ. of Ariz. Press, Tucson, 1992, pp. 557–593.
8. Bell, J. F. I. *et al.*, Near-infrared imaging of Mars from HST: surface reflectance, photometric properties, and implications for MOLA Data. *Icarus*, 1999, **138**, 25–35.
9. Mellon, M. T., Jakosky, B. M., Kieffer, H. H. and Christensen, P. R., High resolution thermal inertia mapping from the Mars global surveyor thermal emission spectrometer. *Icarus*, 2000, **148**, 437–455.
10. Smith, D. E. *et al.*, Mars Orbiter Laser Altimeter–Experiment summary after the first year of global mapping of Mars. *J. Geophys. Res.*, 2001, **106**(E10), 23689–23722.
11. Bibring, J.-P. *et al.*, OMEGA: Observatoire pour le Mine´ralogie, l'Eau, les Glaces et l'Activité, Eur. Space Agency Spec. Publ. *ESA SP*, 2004, **1240**, 37–49.
12. Sun, X., Neumann, G. A., Abshire, J. B. and Zuber, M. T., Mars 1064 nm spectral radiance measurements determined from the receiver noise response of the Mars Orbiter Laser Altimeter. *Appl. Opt.*, 2006, **45**(17), 3960–3971.
13. Heavens, N. G., The reflectivity of Mars at 1064 nm: derivation from Mars Orbiter Lase Altimeter Data and Application to Climatology and Meteorology. *Icarus*, 2016, **289**, 1–21.
14. Kiran Kumar, A. S. and Chauhan, P., Scientific exploration of Mars by first Indian interplanetary space probe: Mars orbiter mission. *Curr. Sci.*, 2014, **107**(7), 1096.
15. Ody, A. *et al.*, Global Maps of anhydrous minerals at the surface of Mars from OMEGA/Mex. *J. Geophys. Res. Planets*, 2012, 188, 10.1029/2012JE004117.
16. Poulet, F. *et al.*, Martian surface mineralogy from Observatoire pour la Minéralogie, l'Eau, les Glaces et l'Activite on board the Mars express spacecraft (OMEGA/MEx): global mineral maps. *J. Geophys. Res.*, 2007, **112**, E08S02, 10.1029/2006JE002840.

ACKNOWLEDGEMENTS. We thank the support and encouragement provided by Shri Tapan Misra, Space Applications Centre (SAC), Ahmedabad, during this study. Support provided by Dr B. S. Gohil, Earth, Ocean, Atmosphere, Planetary Science and Applications Area (EPSA), SAC is thankfully acknowledged. We also thank the sensors and data products teams for providing the MSM data.

Received 29 February 2016; revised accepted 1 March 2017

doi: 10.18520/cs/v113/i01/112-116

Fracture behaviour of fibre reinforced geopolymer concrete

S. Sundar Kumar[1,*], K. C. Pazhani[2] and K. Ravisankar[1]

[1]CSIR-Structural Engineering Research Centre, Taramani, Chennai 600 113, India
[2]Anna University, Adyar, Chennai 600 025, India

Geopolymers have several applications and concrete is one of the materials that can be produced with geopolymer as binder. Since industrial byproducts/wastes such as fly ash, iron slag, micronized biomass silica, silica fume, red mud, etc. can be used as a binder instead of Portland cement, geopolymer concrete (GPC) has generated lot of interest among the scientific and engineering community. This has also resulted in reduced carbon footprint of concrete and an effective method of disposing industrial waste. In this study GPC with a blend of class-f fly ash and ground granulated blast furnace slag as binder has been developed, and its flexural and fracture characteristics have been studied. The GPC developed has a 28-day compressive strength in the range 40–50 MPa. Incorporation of steel fibres resulted in increased flexural strength, enhanced fracture properties and ductility. The residual strength of steel fibre reinforced GPC was also determined in the study.

Keywords: Alkali activators, fracture behaviour, fly ash, geopolymer concrete, iron slag, steel fibres.

CONCRETE is the second most consumed commodity by humans, and Portland cement (PC) has been the binder in concrete for centuries. However, there is also a parallel effort being made to reduce the consumption of cement. Being produced from naturally occurring calcareous and argillaceous materials, cement consumes a lot of energy and causes environmental degradation during excavation and processing of raw materials. In an effort to reduce cement consumption, industrial by-products such as iron slag and fly ash are being used as partial replacement for cement. Incorporation of fly ash and slag not only results in reducing the volume of cement used, but also leads to better quality of concrete. When these supplementary cementitious materials are incorporated in a proper manner, durability of concrete is enhanced without compromising on its strength. The use of slag in cement dates back to the 1940s, when attempts were made to activate slag using alkalis. The bibliographic history of important events in the development of alkali-activated cement has been documented by Li *et al.*[1]. Alkali activation completely eliminates the use of PC, unlike partial replacement of cement with slag or fly ash. In 1979, Davidovits introduced the term 'geopolymer' and defined it as an

*For correspondence. (e-mail: ssk@serc.res.in)

amorphous, three-dimensional, short-range order inorganic polymer that forms when a highly concentrated aqueous alkali hydroxide–silicate solution is added to aluminosilicate raw materials (e.g. metakaolin, fly ash, slag)[2]. The process of geopolymerization has been summarized in three basic steps: (i) dissolution of silica (Si) and alumina (Al) atoms from the source material through the action of hydroxide ions; (ii) transportation or orientation or condensation of precursor ions into monomers and (iii) setting or polycondensation/polymerization of monomers into polymeric structures[3–5]. It has been widely accepted that geopolymer though not a polymer in the true sense, since the polymeric chain is not infinite, can still be brought under the broad domain of inorganic polymers[6]. A major difference during the initial stages of geopolymer concrete (GPC) production is the curing method. When class-f fly ash is used as source material, heat curing becomes a necessity for strength development; however, when a combination of fly ash and ground granulated blast furnace slag (GGBS) is used, then heat curing can be avoided. The calcium that dissolves from the slag significantly influences both early and later age properties, and the availability of free calcium ions prolongs fly ash-dissolution and enhances geopolymer gel formation[7]. Nath and Sarkar[8] have reported a significant improvement in both early age and 28 days strength of fly-ash based geopolymer with addition of 5% ordinary Portland cement (OPC). Coexistence of geopolymeric gel and calcium silicate hydrate (CSH) gel has been reported when a substantial amount of reactive calcium is present initially. The voids and pores within the geopolymeric binder become filled with the CSH gel[9]. This hybrid micro structure leads to higher strength at lower concentration of activators without any special curing methods.

The low tensile and flexural strength of concrete can be substantially increased with incorporation of steel fibres; they not only increase the tensile and flexural strength, but also increase the energy absorption capacity and hence the ductility of concrete. The steel fibres act as micro reinforcement and improve the performance by bridging cracks that develop in concrete at low tensile strain. Steel fibres increase the impact and vibration resistance, and hence are widely used in industrial floors, etc. The bridging efficiency of fibres depends upon the bond strength between the fibres and the matrix they are embedded in. Fracture behaviour of concrete is a well-researched area for more than 40 years. The effect of supplementary cementitious materials such as fly ash, slag, etc. has been extensively documented. There are numerous theories proposed and the principles of fracture 3 mechanics have been incorporated in the codes as well. There is extensive literature available on the fracture behaviour OPC-based concrete[10–16]. Understanding the fracture behaviour of a heterogeneous material like concrete ultimately leads to efficient design of structures. However, when there is change in matrix, it is necessary to evaluate the flexural and fracture behaviour of concrete. Geopolymer binder differs substantially from PC binder in terms of chemical reactions and microstructure formed. There are few studies available in the literature on fracture behaviour of GPC. Pan *et al.*[17] have studied the fracture properties of geopolymer paste and concrete. They have concluded that though the tensile strength of GPC is higher, fracture energy and elastic modulus are lower, and GPC is more brittle than OPC of similar strength. Sarker *et al.*[18] have also reported that the fracture energy of heat cured fly ash-based GPC is similar to that of OPC with higher tensile strength, bond strength and a more brittle behaviour. Ganesan *et al.*[19] have reported an improvement in tension stiffening and cracking characteristics of GPC with the addition of steel fibres. They have also proposed a method for predicting the width of cracks in reinforced GPC elements under uniaxial tension. Rao *et al.*[20] have reported a 25% higher characteristic length for fly Ash and GGBS-based GPC. Hence there is a necessity to develop a large database on material properties of GPC such as elastic modulus, stress–strain behaviour and fracture parameters. In the present study, two fly ash and slag-blended GPC mixes have been developed with low concentration activators and ambient air curing. The concrete mixes were incorporated with hook-shaped steel fibres at a dosage of 60 kg/m^3 of concrete. Fracture, flexural and residual strength parameters have been evaluated for steel fibre reinforced GPC.

A combination of class-f fly ash and GGBS was used as binder in the present study. Table 1 provides the chemical composition of fly ash and GGBS. The final mix proportion of GPC was obtained through various trials mixes. The aim was to obtain concrete with a 28-day average compressive strength in the range 40–50 MPa. In the first mix, 75% class-f fly ash and 25% GGBS were used, whereas the second mix both class-f fly ash and GGBS were used in equal proportion. The river sand used was of finess modulus 2.63. Crushed granite stones of maximum size 12.6 mm were used as coarse aggregates. Activator solution was prepared by dissolving calculated quantity of NaOH flakes in distilled water.

Dissolution of NaOH in water is exothermic; hence the solution was cooled to room temperature and sodium silicate (Table 2) twice by weight (of NaOH) was added to NaOH solution at the time of mixing concrete. Table 3 shows the mix ratio in terms of quantity per cubic metre of concrete. Since the binder adopted was a blend of class-f fly ash and GGBS, the concrete mix did not require any special curing. For the same concrete mix, 60 kg/m^3 of hook-shaped discrete steel fibres were added; the length of the fibre was 25 mm with aspect ratio (l/d) of 55.55. The specimens were air-cured under shade, ensuring no direct exposure to sunlight.

Cubes of 100 mm dimension were used to determine the compressive strength of GPC mixes. Prisms of

Table 1. Chemical composition of binder materials (%)

Material	SiO_2	Al_2O_3	Fe_2O_3	CaO	MgO	Na_2O	K_2O	TiO_2	Mn_2O_3	SO_3
Fly ash	62.10	27.44	4.57	0.83	0.55	0.04	1.17	1.09	0.04	0.40
Slag	43.30	12.40	0.61	40.20	1.40	0.80	0.50	–	–	–

Table 2. Composition of sodium silicate

Specific gravity	Na_2O (%)	SiO_2 (%)	Total solids (%)	Viscosity (N-s/m^2)
1.5	14.20	31.20	45.40	900

Table 3. Geopolymer concrete mix quantity

Mix ID	m1 (kg/cu. m)	m2 (kg/cu. m)
Fly ash	300	203.5
GGBS	100	203.5
Sand	650	634.2
Coarse aggregate	1073	1113
Water	157	175
Sodium hydroxide	40	23.62
Sodium silicate	80	47.24

dimension $100 \times 100 \times 500$ mm were used to conduct three-point bending test and determine fracture parameters. A notch of 25 mm depth was induced during casting of the prism itself at mid span. Hence a_0/h (notch height/beam depth) ratio of 0.25 was maintained for all the specimens. L_0/h (distance between the supports/beam depth) ratio adopted was 4, with a clear span of 400 mm. Figure 1 provides the specimen details and loading arrangements adopted.

The testing was carried out in a 250 tonne servo-controlled universal testing machine under displacement control, and at a loading rate of 0.05 mm/min. The displacement was recorded with a linear variable differential transformer (LVDT) and crack mouth opening displacement (CMOD) measured using a clip gauge. Figure 2 shows a typical test being carried out.

The fracture energy (G_F) was calculated from the principles of 'work of fracture' (criterion I)[21] by using eq. (1)

$$G_f = \frac{w_0 + mg\delta_0}{A_{\text{lig}}}, \tag{1}$$

where W_0 is the area under the load–deflection curve (N–m), m the mass of the beam between the supports (kg), g the acceleration due to gravity (m^2/s), δ_0 the deflection at final failure of the beam (m) and A_{lig} is the area of the ligament (m^2). Critical stress intensity factor (K_{ic}) defined as the stress concentration that exists just in front of the crack tip when the crack starts to propagate, can be calculated using eq. (2) given below

$$K_{ic} = \frac{3Pl}{2bd^2}(\sqrt{a}) * (1.93 - 3.07A + 14.53A^2 - 25.11A^3 + 25.8A^4), \tag{2}$$

where $A = (a/d)$, a is the depth of the notch (mm), d the depth of the beam (mm), b the width of the beam (mm), P the maximum load (N) and l is the span length of the beam (mm).

Fracture energy can also be computed as the area under the stress–displacement curves (criterion II). Assuming a linear stress (σ) distribution over fracture depth; tensile stress was calculated as follows

$$\sigma = \frac{3Fl}{2b(h - a_0)^2}, \tag{3}$$

where F is the load recorded during the three-point bending test. The fracture energy was then evaluated up to a specified displacement according to eq. (4). There are many studies in the literature that specify various displacement limits. However, fracture energy dissipated up to a displacement of 3 mm only is of interest in general design. Hence in this study fracture energy was calculated up to a displacement of 3 mm.

$$G_f = \int_{\delta=0}^{\delta=\delta_{\text{lim}}} \sigma \, \mathrm{d}\delta. \tag{4}$$

Fracture energy was also evaluated using the equation proposed by CEB-FIP model code[21], to estimate the fracture energy of OPC concrete in terms of compressive strength and maximum aggregate size

$$G_f = (0.0469 * D_{\text{max}}^2 - 0.5D_{\text{max}} + 26) * \left(\frac{f_c}{100}\right)^{0.7}, \tag{5}$$

where D_{max} is the maximum aggregate size (mm), f_c the compressive strength of concrete (MPa), α_0 the shape factor of aggregate (1 for rounded aggregates and 1.44 for angular aggregates), and w/c is the water–cement ratio of concrete. Bazant and Becq-Giraduon[22] proposed an equation (eq. (6)) based on a statistical analysis for fracture energy of OPC concrete in terms of compressive strength, maximum aggregate size and water-to-cement ratio of concrete. The equation has a term of water-to-cement

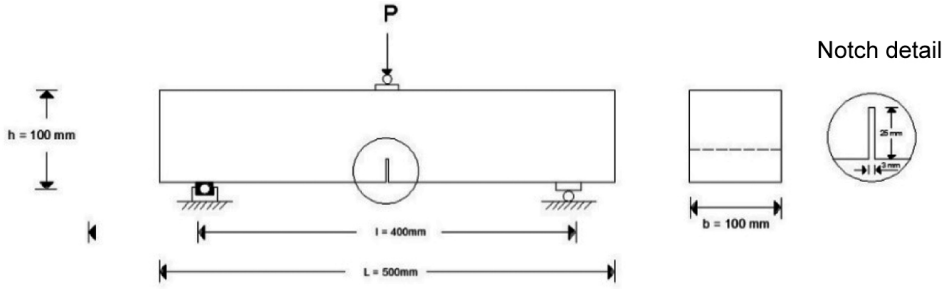

Figure 1. Specimen and loading details for fracture testing.

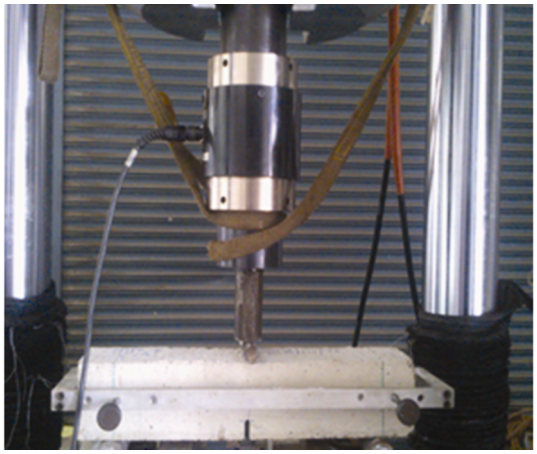

Figure 2. Testing of specimen.

ratio that is relevant to OPC concrete. However Sarker *et al.*[18] have adopted an equivalent liquid-to-binder ratio, the liquid content being the combined mass of sodium hydroxide solution, sodium silicate solution and extra water.

$$G_f = 2.5\alpha_0 \left(\frac{f_c}{0.051}\right)^{0.46} \left(1+\frac{D_{\max}}{11.27}\right)^{0.22} \left(\frac{w}{c}\right)^{-0.30}. \quad (6)$$

Addition of steel fibres in concrete improves its tensile, flexural and residual strength in addition to ductility enhancement. These parameters were evaluated for the fibre reinforced GPC using the equations proposed in RILEM TC 162-TDF[23]. The flexural strength $f_{fct,L}$ was computed up to F_L according to eq. (7), the load at limit of proportionality. F_L is the maximum load recorded up to 0.05 mm mid-point deflection.

$$f_{fct,L} = \frac{3F_L l}{2b(h-a_0)^2}. \quad (7)$$

Equivalent flexural strength $f_{eq,2}$ and $f_{eq,3}$, were evaluated up to a deflection of δ_2 and δ_3 ($\delta_2 = \delta_L + 0.65$ mm and $\delta_3 = \delta_L + 2.65$ mm (where δ_L is the deflection corresponding to F_L) as given in eqs (8) and (9) respectively.

$$f_{eq,2} = \frac{3}{2}\frac{l}{b(h-a_0)^2}\frac{D^f_{BZ,2}}{0.5}, \quad (8)$$

$$f_{eq,3} = \frac{3}{2}\frac{l}{b(h-a_0)^2}\frac{D^f_{BZ,3}}{2.5}. \quad (9)$$

The portion of energy required by fracture of plain concrete D^b_{BZ} was not considered in the evaluation of the equivalent flexural strength. Only the influence of fibres $D^f_{BZ,2}$ and $D^f_{BZ,3}$ was taken into account. The residual flexural tensile strength are calculated at four deflections (at 0.46, 1.31, 2.15 and 3.0 mm) and these are represented by the nos 1, 2, 3, 4 in the nomenclature. According to eq. (10), where b (100 mm), h (100 mm) and l (400 mm) are the width, height and span of the test specimens respectively, and a_0 (25 mm) is the notch depth.

$$f_{R,i} = \frac{3F_{R,i}l}{2b(h-a_0)^2}. \quad (10)$$

Table 4 lists the compressive and flexural strength of GPC mixes. Figures 3 and 4 show typical load versus mid span deflection, and load versus crack mouth opening displacement curves respectively, for each concrete mix tested.

The load deflection behaviour of GPC mixes without steel fibres displayed a linear behaviour up to peak load at which point a crack developed at the notch. Load drop was rapid with high rate of crack propagation. In mixes with fibres, initial curve was linear up to the point of crack initiation. Once crack formation began the slope of load deflection curve changed up to peak load point; post peak when crack depth was nearly half the ligament depth, a near horizontal behaviour was observed in most of the specimens. This can be attributed to bridging action of steel fibres. Once de-bonding or pullout of fibres began softening of curves was observed; however, load drop was gradual indicating good ductility in the specimens. Similar behaviour has been observed in load versus CMOD curves as well. Figure 5 shows a typical crack pattern of the beam specimens.

Table 4. Compressive and flexural strength of geopolymer concrete

Batch	Compressive strength f_c (MPa)	Mean	Standard deviation	Coefficient of variation (%)	Peak load (in flexure) P (kN)	Flexural strength σ_f (MPa)	Mean
m1-1	40.5	40.43	0.90	2.23	3.54	3.78	3.41
m1-2	41.3				3.2	3.41	
m1-3	39.5				2.86	3.05	
m2-1	48.0	46.57	1.56	3.36	5.8	6.19	5.58
m2-2	46.8				4.9	5.23	
m2-3	44.9				5	5.33	
m1-h1	45.5	46.10	0.66	1.42	4.61	4.92	5.14
m1-h2	46.1				5.29	5.64	
m1-h3	46.8				4.55	4.85	
m2-h1	53.1	52.60	1.44	2.74	6.94	7.40	6.54
m2-h2	53.8				5.64	6.02	
m2-h3	51.0				5.81	6.20	

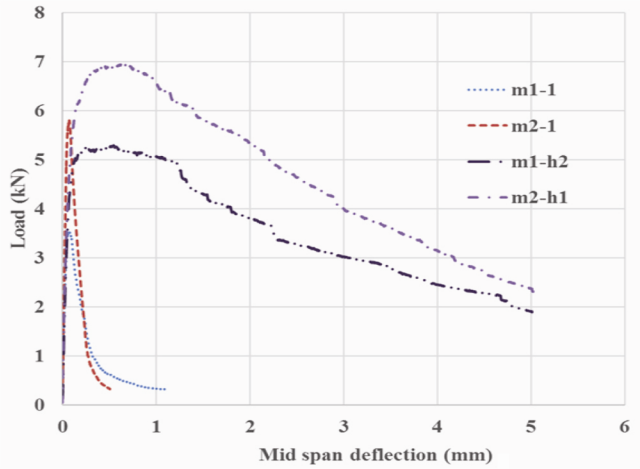

Figure 3. Typical load versus mid span deflection curves (m1 and m2 stand for mix 1 and 2 respectively, h stands for hooked fibres and the last numeric stands for specimen number).

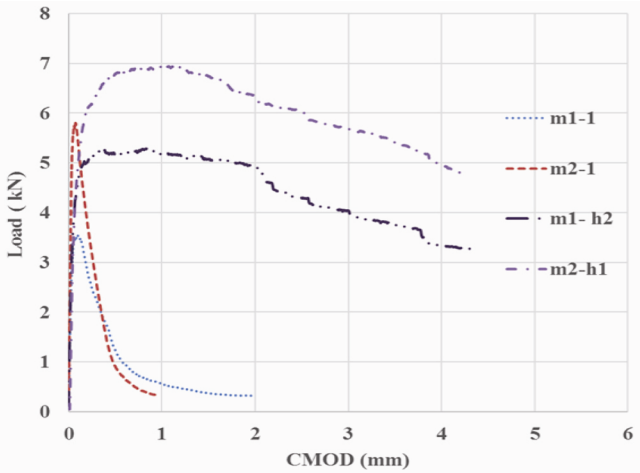

Figure 4. Typical load versus crack mouth opening displacement curves (m1 and m2 stand for mix 1 and 2 respectively, h stands for hooked fibres and the last numeric stands for specimen number).

There was an increase in flexural strength with the incorporation of fibres. For mix m1, the increase was about 50% and for mix m2 it was about 20%. This

Figure 5. Typical crack pattern.

variation could be due to difference in bond strength between the geopolymer matrix and steel fibres, and actual dispersion of fibres at the section of fracture. It was observed that ultimate failure of fiber reinforced specimens was due to pull out, rather than rupture of fibres (Figure 6).

Table 5 shows the fracture parameters calculated. The fracture energy was calculated from the principles of 'work of energy' (criterion I) and that as area under stress–displacement curves (criterion II) was similar for all mixes, with the latter being marginally higher. However, for mixes with fibres this trend was opposite, with fracture energy as per work of energy being marginally higher. The fracture energy reported for fibre reinforced specimens was up to 3 mm deflection only, while for mixes without fibres, energy under the entire curve was reported. Fracture energy evaluated using the equations proposed by CEB-FIP[22], and Bazant and Becq-Giraduon[23] yielded a more conservative value than experimental value. These equations when applied to fibre reinforced concrete yielded a very low value, since they do not consider the contribution of fibres. The fracture energy increased with compressive strength both for mixes with and without fibres. The critical stress intensity factor or fracture toughness, defined as stress just in the vicinity of

Table 5. Fracture parameters for geopolymer concrete

Id	Fracture energy GF (N/m)				Critical stress intensity factor, K_{ic} MPa (–mm$^{0.5}$)
	Criterion (I)	Criterion (II)	Eq (3)	Eq (4)	
m1-1	127.00	138.18	68.39	95.05	8.21
m1-2	138.00	154.10	69.33	95.90	7.42
m1-3	120.00	152.60	67.20	93.96	6.63
Mean	128.33	148.29	68.31	94.97	7.42
m2-1	128.00	140.76	77.03	112.34	13.46
m2-2	121.00	145.00	75.67	111.04	11.37
m2-3	111.00	126.35	73.51	108.94	11.60
Mean	120.00	137.37	75.40	110.77	12.14
m1-h1	1264.00	1389.05	74.19	100.27	10.69
m1-h2	2274.00	1684.76	74.76	100.78	12.27
m1-h3	1008.00	865.95	75.67	101.58	10.56
Mean	1515.33	1313.26	74.88	100.88	11.17
m2-h1	2968.00	2501.23	82.56	117.58	16.10
m2-h2	2253.00	1950.68	83.43	117.58	13.08
m2-h3	2465.00	2226.92	80.36	117.58	13.48
Mean	2562.00	2226.28	82.12	117.58	14.22

Table 6. Flexural strength parameters

	F_L	$f_{fct,l}$	$f_{eq,2}$	$f_{eq,3}$	f_{R1}	f_{R2}	f_{R3}	f_{R4}
a, For geopolymer concrete mixes								
m1-1	3.48	4.64						
m1-2	3.19	4.25						
m1-3	2.59	3.45						
				3.09	*4.11*			
m2-1	5.67	7.56						
m2-2	4.92	6.56						
m2-3	4.92	6.56						
				5.17	*6.89*			
b, For fibre reinforced geopolymer concrete mixes								
m1-h1	4.05	5.40	6.05	4.80	5.89	4.89	3.68	3.32
m1-h2	3.82	5.09	7.25	5.87	6.95	6.15	4.95	4.03
m1-h3	3.85	5.13	4.46	2.95	4.31	2.95	2.08	1.47
	3.91	*5.21*	*5.92*	*4.54*	*5.72*	*4.66*	*3.57*	*2.94*
m2-h1	4.28	5.71	8.94	8.69	9.00	9.12	8.21	7.57
m2-h2	5.28	7.04	7.29	6.68	7.09	6.81	6.13	5.12
m2-h3	5.12	6.83	7.53	7.55	7.21	7.67	7.57	7.15
	4.89	*6.52*	*7.92*	*7.64*	*7.77*	*7.87*	*7.30*	*6.61*

m1 and m2 stands for mix 1 and 2 respectively, h stands for hooked fibres and the italic numeric stands for specimen number.

the crack tip increased substantially with addition of fibres, indicating that a high stress is required for the crack to propogate in fibre reinforced concrete.

Table 6 lists the flexural strength parameters calculated. The equivalent flexural strength decreases as deflection increases. The ratio $f_{eq,2}/f_{eq,3}$ is 0.76 for the mix m1-h (represents the three specimens m1-h1 to m1-h3, and m2-h represents the three specimens m2-h1 to m2-h3), whereas it is 0.96 for m2-h hence there is loss of around 24% and only 4% strength between the deflections δ_2 and δ_3 ($\delta_2 = \delta_L + 0.65$ mm and $\delta_3 = \delta_L + 2.65$ mm where δ_L is the deflection corresponding to F_L, the maximum load recorded up to a midpoint deflection of 0.05 mm) for the respective mixes. The residual strength parameters calculated indicate a decrease in residual strength with increase in deflection; however, a significant strength was retained when the test was stopped as indicated by f_{R4}. The flexural strength parameters indicate the enhanced ductility in the steel fibre reinforced GPC.

Thus, the following can be concluded from the present study.

- Two geopolymer mixes were developed with a blend of class-f fly ash and GGBS and ambient air curing.

Figure 6. Typical failure surface of the beam.

- The geopolymer mixes developed attained a 28-average compressive strength of 40.43 MPa for the mix with 75% fly ash and 25% GGBS as binder, and 46.57 MPa for the mix with fly ash and GGBS in equal proportions.
- Addition of 0.75% steel fibre enhanced the flexural strength by 1.5 and 1.2 times for the mixes m1 and m2 respectively.
- The fracture energy of GPC was found to be directly proportional to compressive strength.
- The fracture surface of GPC specimens was smoother when compared to fracture surface of OPC concrete in general.
- The failure of fiber reinforced concrete specimens was essentially due to pull out and not fibre rupture.
- The post peak behaviour of GPC mixes with steel fibres exhibited an enhanced ductile behaviour with a substantial increase in fracture energy and critical stress intensity factor.
- The reduction in flexural strength (residual strength), post peak, for fibre reinforced mixes was in the range 4%–24% (up to a deflection of 3 mm).
- The flexural and fracture characteristics of GPC are similar to OPC concrete in general. The post-peak performance of GPC can be significantly increased in terms of fracture energy and ductility with the incorporation of steel fibres.

1. Li, C., Sun, H. and Li, L., A review: the comparison between alkali-activated slag (Si + Ca) and metakaolin (Si + Al) cements. *Cem. Concr. Res*., 2010, **40**(9), 1341–1349.
2. Davidovits, J., *Geopolymer Chemistry and Applications*, Institute Geopolymere, Saint-Quentin, France, 2008.
3. Adam, A. A., Strength and durability properties of alkali activated slag and fly ash-based geopolymer concrete Ph D thesis, School of Civil, Environmental and Chemical Engineering, RMIT University, Melbourne, Australia, August 2009.
4. Davidovits, J., Chemistry of geopolymeric systems, terminology. In Proceedings of the 2nd International Conference Geopolymere 99, Saint-Quentin, France, 1999, pp. 9–39.
5. Xu, H. and Van Deventer, J. S. J., The geopolymerisation of alumino-silicate minerals. *Int. J. Miner. Proc.*, 2000, **59**(3), 247–266.
6. Dattatreya, J. K., Bharatkumar, B. H. and Rajamane, N. P., Geopolymer cement concretes – a viable and green alternative to Portland cement based structural concrete. In Proceedings of the 3rd Asian Conference on Ecstasy in Concrete, Chennai, 5–6 December 2010, pp. 243–255.
7. Puligilla, S. and Mondal, P., Role of slag in microstructural development and hardening of fly ash-slag geopolymer. *Cem. Concr. Res.*, 2013, **43**, 70–80.
8. Nath, P. and Sarker, P. K., Effect of GGBFS on setting, workability and early strength properties of fly ash geopolymer concrete cured in ambient condition. *Constr. Build. Mater*., 2014, **66**, 163–171.
9. Yip, Ch. K., Lukey, G. C. and Van Deventer, J. S. J., The coexistence of geopolymeric gel and calcium silicate hydrate at the early stage of alkaline activation. *Cem. Concr. Res.*, 2005, **35**(9), 1688–1697.
10. Bažant, Z. P. and Oh, B. H., Crack band theory for fracture of concrete. *Matér. Struct.*, 1983, **16**(3), 155–177.
11. Tabbara, M. R., Kazeni, M. T. and Pijaudier-Cabot, G., Random particle model for fracture of aggregate or fiber composites. *J. Eng. Mech*., 1990, **116**(8), 1686–1705.
12. Banthia, N. and Sheng, J., Fracture toughness of micro-fiber reinforced cement composites. *Cem. Concr. Compos*., 1996, **18**(4), 251–269.
13. Du, J. *et al.*, Fracture process zone for concrete for dynamic loading. *ACI Mater. J*., 1992, **89**(3), 252–258.
14. Bharatkumar, B. H. *et al.*, Effect of fly ash and slag on the fracture characteristics of high performance concrete. *Mater. Struct*., 2005, **38**(1), 63–72.
15. Raghu Prasad, B. K. *et al.*, Fracture mechanics model for analysis of plain and reinforced high performance concrete beams. *J. Eng. Mech*., 2005, **131**(8), 831–838.
16. Bencardino, F. *et al.*, Experimental evaluation of fiber reinforced concrete fracture properties. *Composites Part B: Eng*., 2010, **41**(1), 17–24.
17. Pan, Z., Sanjayan, J. G. and Vijay Rangan, B., Fracture properties of geopolymer paste and concrete. *Mag. Concr. Res*., 2011, **63**(10), 763–771.
18. Sarker, P. K., Haque, R. and Ramgolam, K. V., Fracture behaviour of heat cured fly ash based geopolymer concrete. *Mater. Des.*, 2013, **44**, 580–586.
19. Ganesan, N., Indira, P. V. and Santhakumar, A., Influence of steel fibres on tension stiffening and cracking of reinforced geopolymer concrete. *Mag. Conc. Res*., 2014, **66**(6), 268–276.
20. Rao, G., *et al.*, Fracture parameters of geopolymer concrete. *Appl. Mech. Mater.*, 2015, **764**, 1090–1094.
21. MC90, Design of concrete structures. CEB-FIP Model Code 1990, 1993.
22. Bazant, Z. P. and Becq-Giraudon, E., Statistical prediction of fracture parameters of concrete and implications for choice of testing standard. *Cem. Concrete Res.*, 2002, **32**, 529–556.
23. RILEM TC 50 – FMC, Determination of the fracture energy of mortar and concrete by means of three-point bend tests on notched beams. *Mater. Struct.*, 1985, **18**, 285–290.

Received 3 May 2016; revised accepted 7 February 2017

doi: 10.18520/cs/v113/i01/116-122